

# Analysis of the Creep Behavior of P92 Steel Welded Joint

Junchao An, Hongyang Jing, Guangchun Xiao, Lei Zhao, and Lianyong Xu

(Submitted May 26, 2010; in revised form October 10, 2010)

Different regions of heat-affected zone (HAZ) were simulated by heat treatment to investigate the mechanisms of the Type IV fracture of P92 (9Cr-2W) steel weldments. Creep deformation of simulated HAZ specimens with uniform microstructures was investigated and compared with those of the base metal (BM) and the weld metal (WM) specimens. The results show that the creep strain rate of the fine-grained HAZ (FGHAZ) is much higher than that of the BM, WM, the coarse-grained HAZ (CGHAZ), and the inter-critical HAZ (ICHAZ). According to the metallurgical investigation of stress-rupture, the FGHAZ and the ICHAZ have the most severely cavitated zones. During creep process, carbides become coarser, and form on grain boundaries again, leading to the deterioration of creep property and the decline of creep strength. In addition, the crack grows along the FGHAZ adjacent to the BM in the creep crack growth test (CCG) of HAZ.

**Keywords** cavity, creep, creep crack growth (CCG), heat-affected zone

of the HAZ on creep properties was also studied. Furthermore, the experimental results are compared with that of the base metal (BM).

## 1. Introduction

Based on the increasing demand for reduction in CO<sub>2</sub> emission, the heat-resistant steels for high-efficient ultra super critical (USC) power plants at 650 °C and above have been paid much attention by scientists in Europe, USA, and Japan (Ref 1-3). However, owing to the inhomogeneous microstructure in the heat-affected zone (HAZ) and fusion line and the lower fracture toughness (compared with the base metal) of the weld metal (WM), most of the fractures in industrial components tend to occur at welded joint (Ref 4-6). Particularly, the HAZ can be divided into three zones with different microstructures: coarse-grained HAZ (CGHAZ), fine-grained HAZ (FGHAZ), and inter-critical HAZ (ICHAZ) adjacent to the BM. Consequently, these microstructural discrepancies usually result in different fracture behaviors in the HAZ.

For high-Cr ferritic steels, such as 9 and 12Cr steels, softening and fine-grained zones, produced in the HAZ of welded joint during the heat cycle of welding, accelerate the evolution of microstructure which will result in damage during elevated temperature creep. It is called Type IV creep, and it will significantly reduce the creep life of welded joint of ferritic steels at elevated temperature and low-stress conditions (Ref 7-15). However, the mechanism responsible for the degradation of creep rupture strength in the welded joint is still not well understood.

The creep rupture tests of simulated HAZ specimens by heat treatments and creep crack growth tests of the P92 (9Cr-2W) steel with tempered lath martensitic structure steel weldment were investigated in the current research. Meanwhile, the effect

## 2. Materials and Methods

### 2.1 Materials and Specimen

The material used in this study is 9Cr-0.4Mo-2W-MnVNb steel (ASME P92), which was cut from a tube of  $\varnothing$  355 mm  $\times$  42 mm. The composition of the P92 alloy (see Table 1) was measured using the Opto-Electronic Direct Reading Spectrometer (OES) (SPECTRO LAB M9). The atomic emission spectrometry (AES) was employed to determine the composition mentioned in the manuscript. The present steel was first normalized at 1040 °C for 4 h, then air-cooled, and finally tempered at 760 °C for 11 h. The Ac<sub>1</sub> and Ac<sub>3</sub> transformation temperatures are 850 and 920 °C, respectively. Gas tungsten arc (GTA) welding and shielded metal arc welding (SMAW) were applied for root pass and fill pass welding, respectively. The actual process parameters of multilayer SMAW welding are given in Table 2.

The standardized CT precracked specimens were adopted in creep crack growth tests based on ASTM E1457-00 (Ref 16). The locations of base metal, WM, and HAZs of the welded joint are shown in Fig. 1. The precrack tip of CT specimen is located in the middle of HAZ.

### 2.2 Heat Treatment for Simulated HAZ

In the actual welded joint, the width of the HAZ is only a few millimeters, and the properties of different regions in the HAZ cannot be derived from welded joint. Hence, it is normal to attempt to simulate the different regions of HAZ microstructure. This can be done either by heat treatment or by weld simulator.

Weld simulator can reflect the changes of microstructure in the HAZ and it is better than heat treatment due to its ability to simulate heating rate accurately and cooling rate of HAZ in the

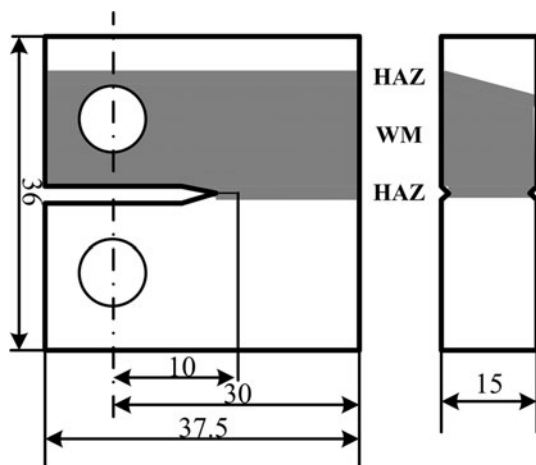
Junchao An, Hongyang Jing, Guangchun Xiao, Lei Zhao, and Lianyong Xu, School of Material Science and Engineering, Tianjin University, Tianjin, China. Contact e-mail: xulianyong@tju.edu.cn.

**Table 1 Chemical composition of P92 steels (wt.%)**

C	Si	Mn	S	P	Cr	Ni	Mo	W	V	Nb	B	Al	N
0.1	0.47	0.4	0.001	0.0082	8.77	0.12	0.38	1.48	0.16	0.054	0.0011	0.02	0.043

**Table 2 Process parameters of multilayer SMAW welding**

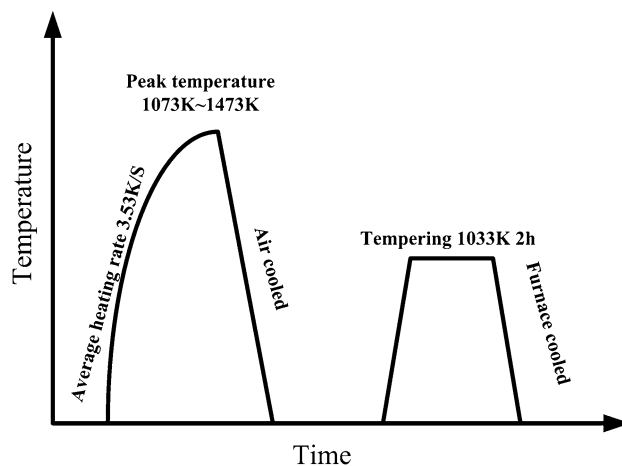
Groove	Single bevel 20°
Preheating	200 °C
Welding current	120 A
Arc voltage	24 V
Welding speed	2.2-2.4 mm/s
Multi-layer	78 pass

**Fig. 1** The geometry and size of the CT specimen used for testing

center of the specimen as well as the really experience. However, it should be noted that the simulated results are dependent on the dimensions of the specimen, and the reasonable width of specimen is 10-15 mm. Therefore, since the size of the simulated zone is limited, it is difficult to extract specimens with uniform microstructure from the HAZ produced using a simulator (Ref 11).

For using heat treatment to simulate the HAZ microstructure, the material is heated rapidly in a furnace to the peak temperature during welding, and then is cooled quickly. Results from HAZ simulated by heat treatments have shown that FGHAZ/ICHAZ is heated to a temperature close to the  $A_{c3}$  temperature of the steel, The Type IV cracking would take place in the welded joint, and has the minimum creep strength (Ref 17). Although the heating and cooling rates that can be achieved are lower than those in an actual weld thermal cycle, furnace heating can heat the whole specimen to the same temperature homogeneously. Thus, the microstructure is uniform throughout the specimen.

Figure 2 shows the condition of heat treatment for the preparation of simulated HAZ specimens. The  $A_{c1}$  temperature of P92 steel is about 850 °C (1093 K), while the  $A_{c3}$  temperature is about 920 °C (1193 K). At an average heating rate of 3.53 K/s, the simulated HAZ specimens were kept for 180 s at various peak temperatures between 850 °C (1073 K) and 1200 °C (1473 K) and then were cooled in air. Finally, the tempering was carried out for each specimen including the BM

**Fig. 2** Test condition of heat treatment for simulated HAZ specimens

at 760 °C (1033 K) for 2 h. The welded joint was prepared by means of multilayer SMAW welding.

### 2.3 Uniaxial Tensile Creep Test and Creep Stress-Rupture Test

To investigate the microstructure evolution and the creep deformation properties of HAZ, uniaxial tensile creep tests for simulated HAZ were conducted on round-bar specimens of 10 mm in diameter and 100 mm in gage length according to ASTM E 139 (Fig. 3). The creep tests for WM and BM were also conducted using the same geometric specimens. The temperature of the creep test was 650 °C, and the applied stress was 160 MPa. The creep stress-rupture test was performed at 650 °C for up to 4032 h, and then it was stopped to investigate the microstructure using an optical microscope.

### 2.4 Creep Crack Growth Test

The creep crack growth tests of welded joint were carried out using CT specimens of 15-mm thickness (see Fig. 1). The notch tip was located in HAZ. The precrack of 2.1 mm was introduced by fatigue loading at room temperature. After fatigue precracking, 25% side-groove of the thickness was machined. The creep crack propagation was measured by the direct-current electrical potential method (Ref 18, 19). Meanwhile, the crack opening displacement in front of the crack tip was also measured. The applied initial stress intensity factor ( $K_I$ ) was 12 MPa  $m^{1/2}$ , and the test temperatures were the same as those used in the creep rupture tests.

## 3. Results and Discussion

### 3.1 Creep Properties and Microstructure Investigation

Figure 4 shows the corresponding creep deformation characteristics of the BM, ICHAZ, FGHAZ, CGHAZ, and the WM

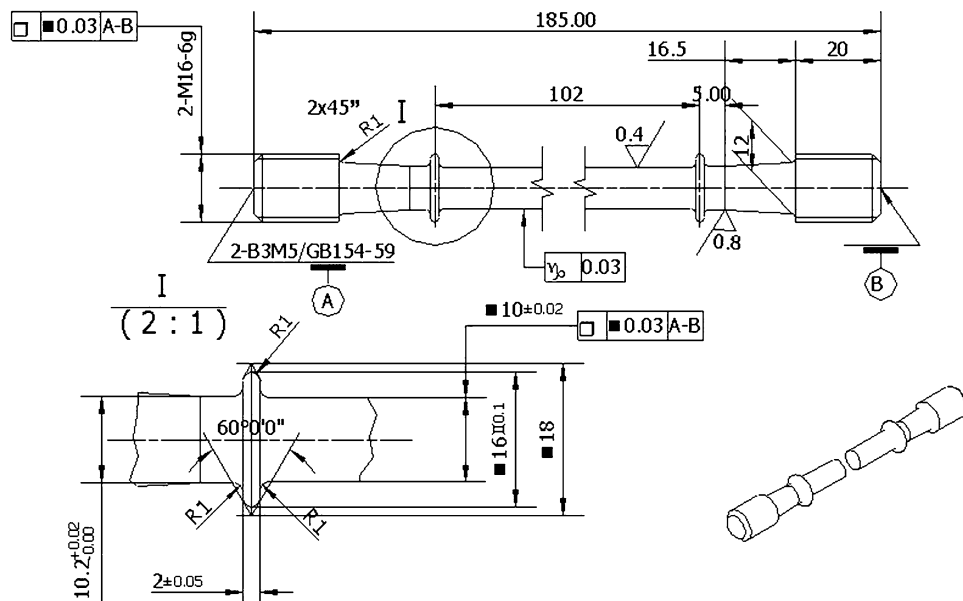


Fig. 3 Dimension of the creep specimen

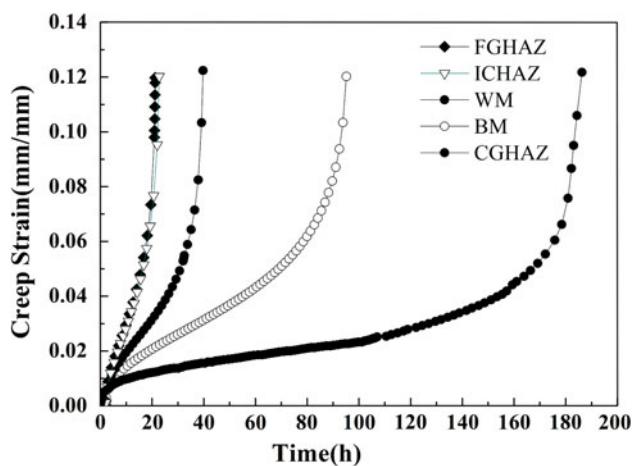


Fig. 4 The creep curves of different regions at 650 °C under 160 MPa

of the P92 steel under the temperature of 650 °C, and the applied stress was 160 MPa. The minimum creep strain rates for the different regions in the welded joint are given in Table 3. The results showed that the creep strain rate of the FGHAZ was much higher than that of the BM and other different zones of HAZ. The creep life of the HAZ simulated at the peak temperature of 1200 °C (CGHAZ) was longer than those of the ICHAZ, FGHAZ, BM, and WM, indicating that the creep strength of the CGHAZ in an actual weld is the highest. The creep life of the FGHAZ was the shortest, while the creep life of the CGHAZ was the longest. The fracture of the welded joint tended to initiate in the FGHAZ.

The interrupted creep stress-rupture test showed that the fracture tend to occur in the FGHAZ and ICHAZ (shown in Fig. 5). A significant number of creep cavities were observed in the FGHAZ and the ICHAZ. After creep rupture test, the FGHAZ is the most severely cavitated zone; the cavitation in the ICHAZ is less than that in the FGHAZ, but much more than

Table 3 The minimum creep rate of different regions of welded joint

Different regions of welded joint	Minimum creep rate, mm/h
FGHAZ	2.78E-3
ICHAZ	2.71E-3
WM	1.21E-3
BM	5.30E-4
CGHAZ	1.33E-4

that in other zones. Meanwhile, there are a few cavitations in the WM. The BM is slightly cavitated, mainly along with grain boundaries, whereas the cavitations in the CGHAZ are less than the WM. It is possible to find exceptional areas with a few relatively large cavities (0.5-1 μm).

TEM micrographs of thin foils cut out from the HAZ adjacent to BM are shown in Fig. 6, to investigate the changes of precipitation of carbides and sub-grain structures before and after creep test (at 650 °C for 4032 h). It showed that carbides were coarser and were mainly located at the grain boundaries. Dislocation densities inside the grains were very low (Fig. 6a). Some of the carbides gathered at grain boundaries, even located at the intersection of three grain boundaries as shown in Fig. 6(b) and (c). TEM micrographs of the extracted replica of the HAZ adjacent to BM of the welded joint for virgin condition and after creep were shown in Fig. 7. The amount of carbide precipitates was little in the virgin condition (Fig. 7a). The precipitated particles observed were  $M_{23}C_6$  and fine MX carbonitrides (Fig. 7b). On the other hand, in the ruptured specimens (Fig. 7c, d), the amount of carbide precipitates was larger, and the size of carbides was coarser than those in the virgin condition (Fig. 7a, b). The precipitation of coarse Laves phase (Fig. 7d) was also observed, though it was not observed in the virgin condition.

In the virgin specimen, these carbides dispersed in the grains can strengthen the matrix, based on the mechanisms of solid solution strengthening and the precipitation hardening, thereby



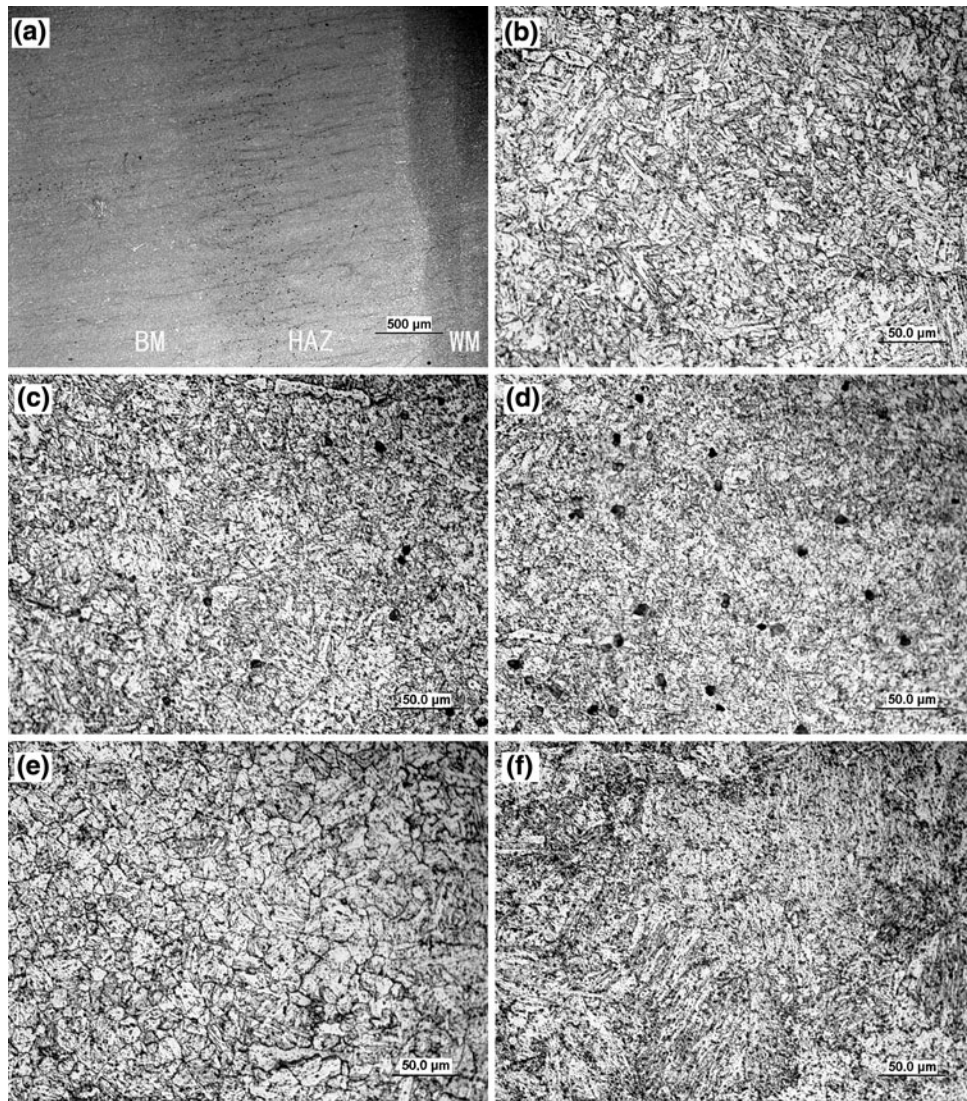


**Fig. 5** The microstructures of different zones of welded joint after creep stress-rupture test: (a) cross section of welded joint, (b) BM, (c) ICHAZ, (d) FGHAZ, (e) CGHAZ, and (f) WM

insuring the creep resistant strength of P92 steel. However, after creep test, carbides become coarser and form on grain boundaries again. This will lead to the deterioration of creep property and the decline of creep strength, along with the decreasing effects of solid solution strengthening and precipitation strengthening. Meanwhile, these coarse precipitates can weaken the bonding force between grain boundaries and the bonding force between the particle and matrix. It can be confirmed that Laves phase tends to precipitate on the grain boundaries. The precipitation strengthening effect from Laves phase is believed to be insignificant as the Mo and W elements are removed from solution in the ferrite, offsetting any beneficial effects of the Laves phase attained with precipitation strengthening resulting in the declines of creep resistance values (Ref 20). Hence, it makes the creep voids apt to nucleate during creep, which leads to further decline of creep resistance strength.

### 3.2 Creep Crack Growth Properties of Welded Joint

The  $C^*$  integral introduced by Riedel and Rice (Ref 21), having been regarded as the most appropriate one among the

existing high temperature fracture parameters, has been widely used to correlate the data of creep crack growth (CCG). In practice, the  $C^*$  parameter can be determined in terms of the measured load line displacement rate, which is needed frequently in crack assessment of the welded structures. In CCG studies of welded joint (Ref 22, 23), the experimental  $C^*$  estimation equation of ASTM E1457 (Ref 16) has been generally applied.

The creep crack growth rate is evaluated by  $C^*$  parameter which is calculated as follows:

$$C^* = \frac{p\Delta_c}{WB_N} \frac{n}{n+1} \left( \frac{2}{1-a/w} + 0.522 \right) \quad (\text{Eq 1})$$

where  $W$  is the specimen width,  $a$  is the crack length,  $P$  is the load,  $B_N$  is the net thickness,  $\Delta_c$  is the crack opening displacement rate, and  $n$  is the creep exponent in Norton's rule.

Figure 8 shows the creep crack growth curves of CT specimens for the welded joint tested at the load that initial  $K_I$  is  $12 \text{ MPa m}^{1/2}$ . Creep crack has propagated on the grain boundaries in the FGHAZ zone heated around the  $A_{c3}$  temperature during welding. As shown in the creep crack

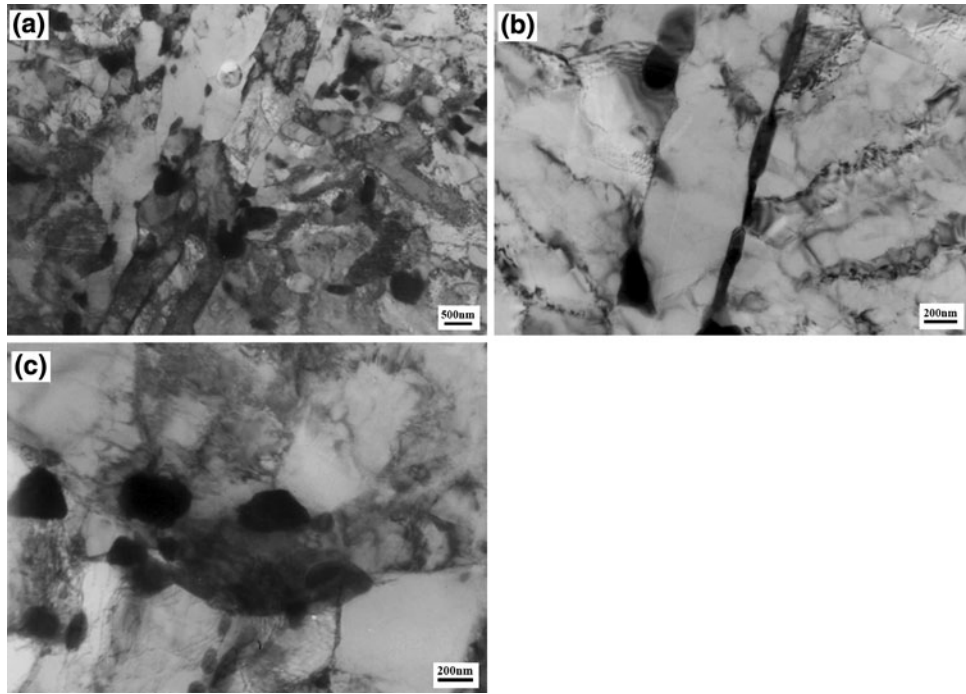


**Fig. 6** Transmission electron micrographs of HAZ adjacent to the base metal. (a) Dislocation densities and carbides, (b) carbides at the grain boundaries, and (c) carbides at the intersection of three grain boundaries

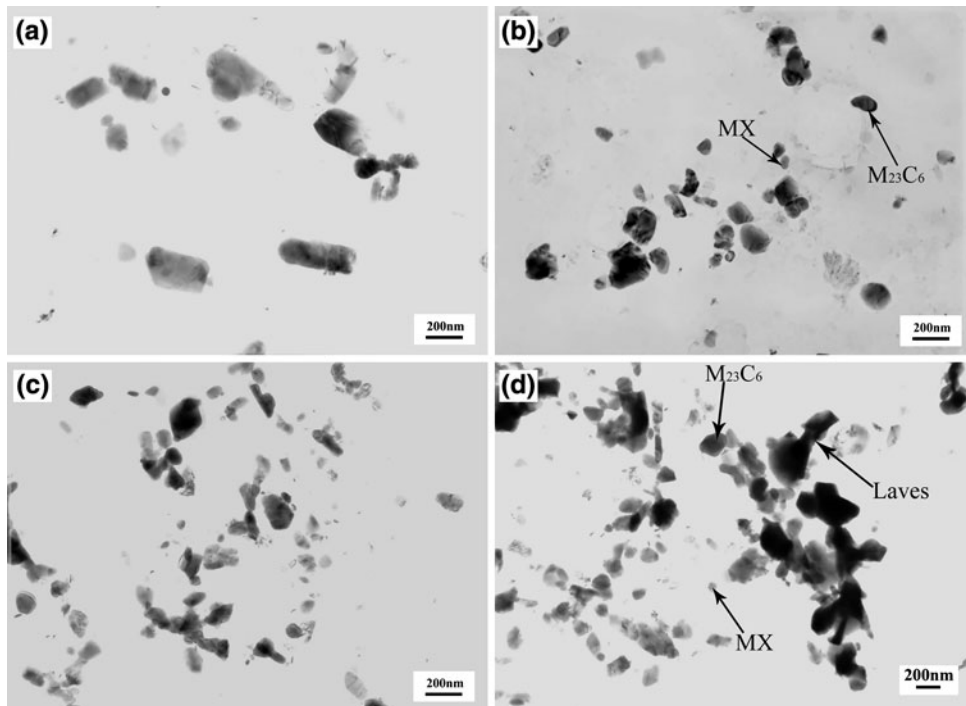


**Fig. 7** Transmission electron micrographs of carbon extraction replicas on the HAZ adjacent to the BM. (a, b) virgin condition and (c, d) creep for 4032 h specimen

growth curves of the welded joint, the crack scarcely grows during incubation period and then grows rapidly during the accelerating stage.

In order to obtain a reliable crack growth data, it is necessary to stop tests before specimen is ruptured. In Fig. 9, the

experimental data of CCG rate was correlated with crack tip parameters. The CCG rates correlate well with  $C^*$ , particularly at higher crack growth rates. It is worth noting that the weldment deformation is inhomogeneous due to microstructure heterogeneity. Crack growth may also follow some



microstructure components that are different from the simulated material on which mechanical and creep data are obtained. Crack growth increases slowly at first and as a result, the region, where the data are concentrated near the lowest  $da/dt$  values, occupies 80-90% of the total creep fracture life, as shown in Fig. 9. The results indicate that the creep deformation and fracture are substantially influenced by inhomogeneous microstructure in terms of their creep properties.

Figure 10 shows micrographs of the creep crack growth of HAZ specimens. Metallographic observation shows that both initial and final crack tips were found in the HAZ, indicating that the defect-propagated regions were throughout the test within the HAZ. For P92 steel, although the initial tip position

was in the middle of the HAZ or closer to the coarse grain region, the crack propagation path was found in the fine grain region adjacent to the BM (see in Fig. 10a). This means that, for longer test duration, the crack could grow in the Type IV position. Many cavities were observed around the crack tip from higher magnification SEM images (Fig. 10b, c), which would result in stress relaxation and acceleration of creep crack growth rate. In Fig. 10(b), it can be observed that the separate cavities first formed, and then coalesced into aligned cavity chains. With the creep duration increasing, cavity chains coalesced into small scale microcracks, and finally formed macroscopic cracks that can be detected in the standard nondestructive inspections.

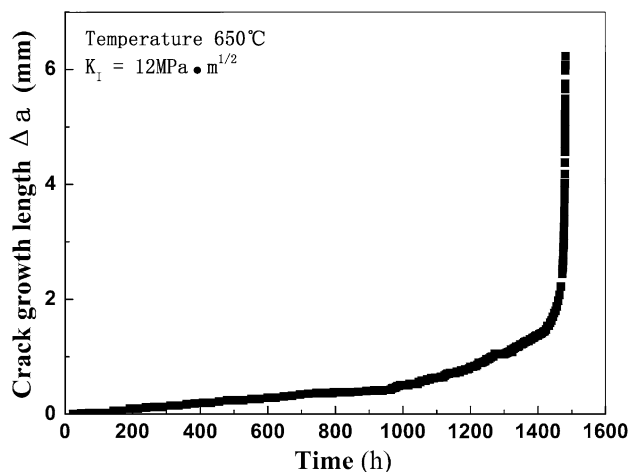


Fig. 8 Creep crack growth curves of CT specimens for welded joint

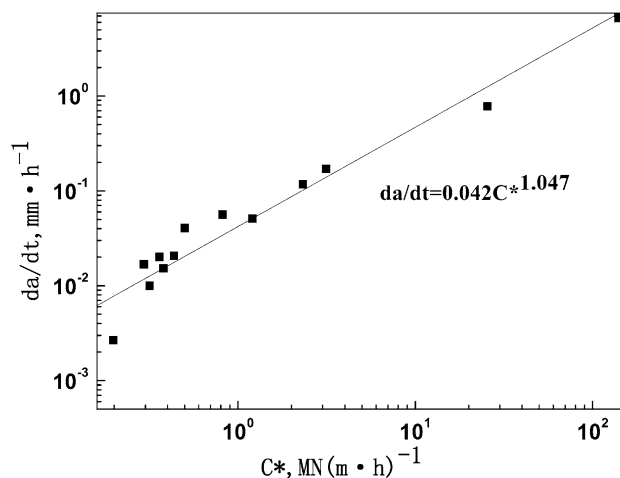


Fig. 9 The relationship between creep crack growth rate and  $C^*$  parameter for P92 welded joint

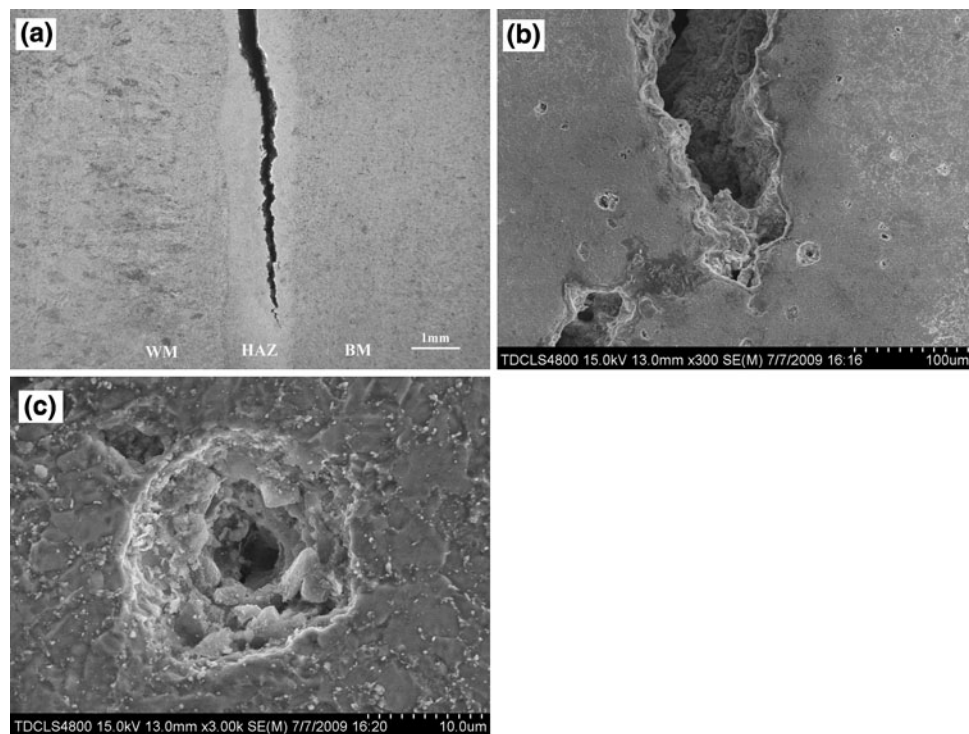


Fig. 10 Creep crack growth path of P92 HAZ specimen. (a) Creep crack growth path, (b) high magnification image of crack tip, and (c) cavity at the crack tip around

## 4. Conclusions

Creep test of the HAZs, creep stress-rupture, and creep crack growth of P92 (9Cr-2W) steel welded joint were investigated, and the following conclusions can be drawn:

1. With respect to the creep deformation characteristics of P92 steel under the temperature of 650 °C, for simulated HAZ specimens, the creep strain rate of fine-grained HAZ was much higher than that of the BM, WM and other different zones of HAZ. The fracture of the welded joint specimen will occur in the FGHAZ.
2. Based on metallurgical investigation of creep stress-rupture test, the FGHAZ have the most severely cavitated zones where crack initiation and growth are easier. In the industrial practice, Type IV creep fracture will occur. During creep process, carbides become coarser and form on grain boundaries again. This will lead to the deterioration of creep property and the decline of creep strength.
3. The crack growth rate of welded joint correlates well with  $C^*$ , particularly at higher crack growth rates. The first stage of creep crack growth curve (lower crack growth rates) accounts for 80-90% of the total creep fracture life. The creep-propagated position of HAZ specimen is located at the fine grain region adjacent to the base metal.

## Acknowledgment

The authors acknowledge the research funding and support by National Natural Science Foundation for Youth of China (Grant No. 50805103), Tianjin Nature Science Foundation of China (Grant No. 08JCZDJ18100), Tianjin Nature Science Foundation of China (Grant No. 08JCYBJC09100) and New Teacher Project in Doctor sites Foundation of China Ministry of Education (Grant No. 20070056096).

## References

1. R. Blum and R.W. Vanstone, Materials Development for Boilers and Steam Turbines Operating at 700 °C, *Proceedings of the Sixth International Charles Parsons Turbine Conference*, September 16–18, 2003 (Dublin, Ireland), 2003, p 489–510
2. R. Viswanathan, J.F. Henry, J. Tanzosh, G. Stanko, J. Shingledecker, and B. Vitalis, US Program on Materials Technology for USC Power Plants, *Proceedings of the Fourth International Conference on Advances in Materials Technology for Fossil Power Plants*, 25–28 October 2004 (Hilton Head Island, South Carolina, USA), 2004, p 3–19
3. F. Abe, H. Okada, S. Wanikawa, M. Tabuchi, T. Itagaki, K. Kimura, K. Yamaguchi, and M. Igarashi, Guiding Principles for Development of advanced Ferritic Steels for 650 1C USC Boilers, *Proceedings of the Seventh Liege Conference on Materials for Advanced Power Engineering 2002*, 30 September–2 October, 2002 (Liege, Belgium), 2002, p 1397–1406
4. M.E. Kassner and T.A. Hayes, Creep Cavitation in Metals, *Int. J. Plast.*, 2003, **19**(10), p 1715–1748
5. J.H. Kim, Y.J. Oh, I.S. Hwang, D.J. Kim, and J.T. Kim, Fracture Behavior of Heat-Affected Zone in Low Alloy Steels, *J. Nucl. Mater.*, 2001, **299**(2), p 132–139
6. D.M. Rodrigues, L.F. Menezes, and A. Loureiro, The Influence of the HAZ Softening on the Mechanical Behaviour of Welded Joints Containing Cracks in the Weld Metal, *Eng. Fract. Mech.*, 2004, **71**(13–14), p 2053–2064
7. F. Abe and M. Tabuchi, Microstructural and Creep Strength of Welds in Advanced Ferritic Power Plant Steels, *Sci. Technol. Weld. Join.*, 2004, **9**, p 22–30
8. E. Letofsky and H. Cerjak, Metallography of 9Cr Steel Power Plant Weld Microstructures, *Sci. Technol. Weld. Join.*, 2004, **9**, p 31–36
9. Y. Hasegawa, M. Ohgami, and Y. Okamura, Creep Properties of Heat Affected Zone of Weld in W Containing 9-12% Chromium Creep Resistant Martensitic Steels at Elevated Temperature. *Advanced Heat Resistant Steels for Power Generation*, IOM Communications, The University Press, Cambridge, 1999, p 655–667
10. M. Tabuchi, T. Watanabe, K. Kubo, M. Matsui, J. Kinugawa, and F. Abe, Microstructure and Creep Strength of Welded Joints for W Strengthened High Cr Ferritic Steel, *J. Soc. Mater. Sci.*, 2001, **50**, p 116–121 (in Japanese)
11. M. Tabuchi, T. Watanabe, K. Kubo, M. Matsui, J. Kinugawa, and F. Abe, Creep Crack Growth Behavior in the HAZ of Weldments of W Containing High Cr Steel, *Int. J. Pres. Ves. Pip.*, 2001, **78**, p 779–784
12. M. Matsui, M. Tabuchi, T. Watanabe, K. Kubo, J. Kinugawa, and F. Abe, Degradation of Creep Strength in Welded Joint of 9-12%Cr Steels, *ISIJ Int.*, 2001, **41**, p S126–S130
13. M. Tabuchi, M. Matsui, T. Watanabe, H. Hongo, K. Kubo, and F. Abe, Creep Fracture Analysis of W Strengthened High Cr Steel Weldment, *Mater. Sci. Res. Int.*, 2003, **9**, p 23–28
14. T. Watanabe, M. Yamazaki, H. Hongo, M. Tabuchi, and T. Tanabe, Effect of Stress on Microstructural Change Due to Aging at 823 K in Multilayer Welded Joint of 2.25Cr-1Mo Steel, *Int. J. Pres. Ves. Pip.*, 2004, **81**, p 279–284
15. T. Watanabe, Relationship Between Type IV Fracture and Microstructure on 9Cr-1Mo-V-Nb Steel Welded Joint Creep-Ruptured After Long Term, *Tetsu-to-Hagane*, 2004, **90**, p 206–212 (in Japanese)
16. ASTM E1457-00, Standard Test Method for Measurement of Creep Crack Growth Rates in Metals, *Annual Book of ASTM Standards*, Vol 3 (No. 1), 2001, p 936–950
17. S.K. Albert, M. Matsui, H. Hongo, T. Watanabe, K. Kubo, and M. Tabuchi, Creep Rupture Properties of HAZs of a High Cr Ferritic Steel Simulated by a Weld Simulator, *Int. J. Pres. Ves. Pip.*, 2004, **81**(3), p 221–234
18. H.H. Johnson, Calibrating the Electric Potential Method for Studying Slow Crack Growth, *Mater. Res. Stand.*, 1965, **5**, p 442–445
19. K.H. Schwalbe and D. Hellmann, Application of the Electrical Potential Method to Crack Length Measurements Using Johnson's Formula, *J. Test. Eval.*, 1980, **9**(4), p 218–220
20. P.J. Ennis, A. Zielinska-Lipiec, O. Wachter, and A. Czyska-Filemonowicz, Microstructural Stability and Creep Rupture Strength of the Martensitic Steel P92 for Advanced Power Plant, *Acta Mater.*, 1997, **45**, p 4901
21. H. Riedel and J.R. Rice, Tensile Cracks in Creeping Solids Fracture Mechanics, *Fracture Mechanics: Twelfth Conference*, ASTM STP 700, American Society for Testing and Materials, 1980, p 112–130
22. B. Dogan and B. Petrovski, Creep Crack Growth on High Temperature Weldments, *Int. J. Pres. Ves. Pip.*, 2001, **78**, p 795–805
23. L. Allais, J.P. Dessalas, T. Forgeron et al., Creep Behaviour of Full-Size Welded Joints: Defect Acceptance Criteria, *Fatig. Fract. Eng. Mater. Struct.*, 1998, **21**, p 791–803